Hybrid Kalman Filter: A New Approach for Aircraft Engine In-Flight Diagnostics

Takahisa Kobayashi
ASRC Aerospace Corporation, Cleveland, Ohio

Donald L. Simon
U.S. Army Research Laboratory, Glenn Research Center, Cleveland, Ohio

NASA STI Program . . . in Profile

Since its founding, NASA has been dedicated to the advancement of aeronautics and space science. The NASA Scientific and Technical Information (STI) program plays a key part in helping NASA maintain this important role.

The NASA STI Program operates under the auspices of the Agency Chief Information Officer. It collects, organizes, provides for archiving, and disseminates NASA's STI. The NASA STI program provides access to the NASA Aeronautics and Space Database and its public interface, the NASA Technical Reports Server, thus providing one of the largest collections of aeronautical and space science STI in the world. Results are published in both non-NASA channels and by NASA in the NASA STI Report Series, which includes the following report types:

- TECHNICAL PUBLICATION. Reports of completed research or a major significant phase of research that present the results of NASA programs and include extensive data or theoretical analysis. Includes compilations of significant scientific and technical data and information deemed to be of continuing reference value. NASA counterpart of peer-reviewed formal professional papers but has less stringent limitations on manuscript length and extent of graphic presentations.

- TECHNICAL MEMORANDUM. Scientific and technical findings that are preliminary or of specialized interest, e.g., quick release reports, working papers, and bibliographies that contain minimal annotation. Does not contain extensive analysis.

- CONTRACTOR REPORT. Scientific and technical findings by NASA-sponsored contractors and grantees.

- CONFERENCE PUBLICATION. Collected papers from scientific and technical conferences, symposia, seminars, or other meetings sponsored or cosponsored by NASA.

- SPECIAL PUBLICATION. Scientific, technical, or historical information from NASA programs, projects, and missions, often concerned with subjects having substantial public interest.

- TECHNICAL TRANSLATION. English-language translations of foreign scientific and technical material pertinent to NASA's mission.

Specialized services also include creating custom thesauri, building customized databases, organizing and publishing research results.

For more information about the NASA STI program, see the following:

- Access the NASA STI program home page at *http://www.sti.nasa.gov*

- E-mail your question via the Internet to *help@sti.nasa.gov*

- Fax your question to the NASA STI Help Desk at 301–621–0134

- Telephone the NASA STI Help Desk at 301–621–0390

- Write to:
  NASA Center for AeroSpace Information (CASI)
  7115 Standard Drive
  Hanover, MD 21076–1320

U.S. ARMY
ARL
RESEARCH LABORATORY

Hybrid Kalman Filter: A New Approach for Aircraft Engine In-Flight Diagnostics

Takahisa Kobayashi
ASRC Aerospace Corporation, Cleveland, Ohio

Donald L. Simon
U.S. Army Research Laboratory, Glenn Research Center, Cleveland, Ohio

Acknowledgments

Level of Review: This material has been technically reviewed by technical management.

Hybrid Kalman Filter:
A New Approach for Aircraft Engine In-Flight Diagnostics

Takahisa Kobayashi
ASRC Aerospace Corporation
Cleveland, Ohio 44135

Donald L. Simon
U.S. Army Research Laboratory
Glenn Research Center
Cleveland, Ohio 44135

Abstract

In this paper, a uniquely structured Kalman filter is developed for its application to in-flight diagnostics of aircraft gas turbine engines. The Kalman filter is a hybrid of a nonlinear on-board engine model (OBEM) and piecewise linear models. The utilization of the nonlinear OBEM allows the reference health baseline of the in-flight diagnostic system to be updated to the degraded health condition of the engines through a relatively simple process. Through this health baseline update, the effectiveness of the in-flight diagnostic algorithm can be maintained as the health of the engine degrades over time. Another significant aspect of the "hybrid" Kalman filter methodology is its capability to take advantage of conventional linear and nonlinear Kalman filter approaches. Based on the hybrid Kalman filter, an in-flight fault detection system is developed, and its diagnostic capability is evaluated in a simulation environment. Through the evaluation, the suitability of the hybrid Kalman filter technique for aircraft engine in-flight diagnostics is demonstrated.

Introduction

In-flight diagnostics of aircraft gas turbine engines is a critical task for improving engine operation. The capability to detect and/or isolate any faults can not only improve the safety and efficiency of engine operation during flight but also facilitate better maintenance planning. Since diagnostic system results can influence the follow-on actions taken by the maintenance crew, flight crew, or control system, it is critical that they be highly reliable. In-flight diagnostic systems, therefore, must be designed with robustness to non-fault-related factors which exist in the real environment and can potentially mislead diagnostic systems to generate incorrect results.

In-flight diagnostic systems are, in general, designed at a nominal health, or non-degraded, condition. This design condition becomes a reference health baseline for diagnostics; any observed deviations in engine outputs from their reference condition values may indicate the presence of a fault. In-flight diagnostic systems can perform effectively as long as the health of the real engine remains in the vicinity of the reference health baseline, thereby making engine output deviations prominent when a fault takes place.

As the real engine degrades over time, in-flight diagnostic systems may lose their effectiveness. Engine health degradation is a normal aging process that occurs in all aircraft engines due to usage and therefore is not considered as a fault. However, similar to various faults, degradation causes the engine outputs to deviate from their reference condition values. When engine output deviations eventually exceed a certain level, the diagnostic system may misinterpret the health degradation as a fault and consequently generate a false alarm.

One approach to maintaining the effectiveness of in-flight diagnostic algorithms, when applied to degraded engines, is to periodically update or re-design the diagnostic algorithms based on the estimated amount of health degradation. Health degradation can be estimated by trend monitoring systems using post-flight data [1-3]. Through the update based on the estimated health degradation, the health baseline of an in-flight diagnostic system can be shifted to the vicinity of the degraded engine, and thereby the system is able to effectively diagnose the presence of a fault. One issue with this approach is its practicality. Depending on the complexity of the diagnostic algorithms, the update process may take too much time and thus may be impractical.

To address the above issue, a uniquely structured Kalman filter was developed in Reference [4] for application to in-flight diagnostics of aircraft gas turbine engines. This Kalman filter is called a "hybrid" Kalman filter (HKF) because of its hybrid structure; it is composed of a nonlinear on-board engine model (OBEM) and piecewise linear state-space models which include Kalman gain matrices. With this architecture, the system update to account for engine health degradation is achieved through a relatively simple process: by feeding the estimated health degradation values into the OBEM. The linear component of the hybrid Kalman filter, namely the linear engine models and associated Kalman gains, does not need to be updated though the degradation of the real engine progresses with time.

In the following sections of this paper, the problem setup for in-flight diagnostics and the design approach of the HKF, described in Reference [4], are given. Then the design

methodology is applied to a large commercial aircraft engine model, and the functionality of the HKF is investigated. Based on the HKF, an in-flight fault detection system is developed. Its performance at detecting faults in sensors, actuators, and component while avoiding false alarms is evaluated in a simulation environment.

Problem Setup for In-Flight Diagnostics

The primary objective of an in-flight diagnostic system is to detect faults as early as possible from the observed engine outputs while avoiding false alarms and missed detections. After the detection of a fault, the identity or severity of the detected fault must be classified through the fault isolation process. False alarms can misguide the maintenance crew, flight crew, or control system into taking inappropriate actions; therefore it is critical to avoid them. Since false alarms are the result of misinterpretation of non-fault-related factors, it is important to understand the influence of such factors on engine outputs.

Engine health degradation is one of the non-fault-related factors that can cause false alarms. As shown in Figure 1, engine health degradation is described as the gradual deviation of health parameters from the initial healthy baseline. Health parameters are efficiencies and flow capacities of engine components such as compressors and turbines, and they indicate the health of such components. As they deviate from the initial healthy baseline, engine outputs will also deviate from their nominal condition values. Since degradation is a normal aging process that all aircraft engines will experience due to usage, it is not considered as a fault, whereas an abnormal and unexpected event is a fault. However, as the engine output deviations increase due to the gradual progression of health degradation, it becomes difficult to distinguish the presence of faults from health degradation through the observation of engine outputs. As a result, an in-flight diagnostic system loses its effectiveness as the engine degrades over its lifetime. An example of such loss of diagnostic effectiveness due to health degradation is shown in References [5,6] for the case of sensor fault diagnostics based on Neural Networks.

To reduce the influence of health degradation on in-flight diagnostic performance, the diagnostic system needs to be
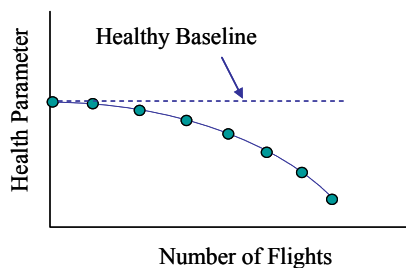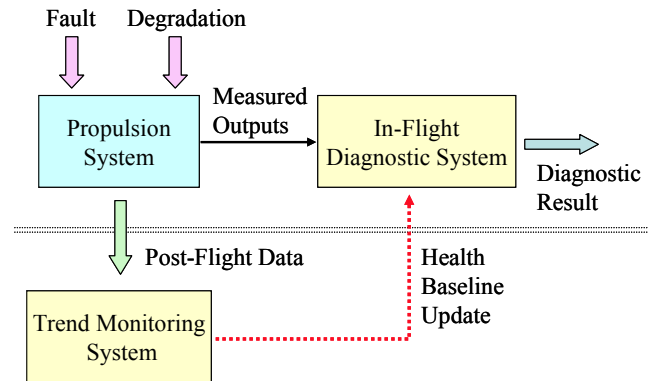

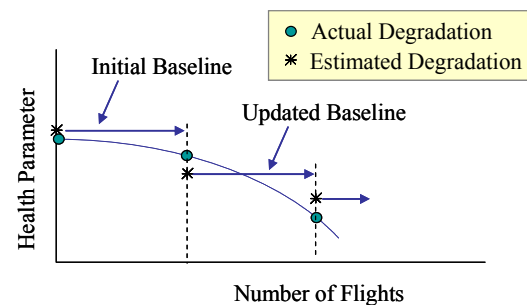Figure 2.–Process of Health Baseline Update.

Figure 3.–Baseline Update Using Estimated Health Degradation.

updated periodically based on the estimated amount of health degradation, as shown in Figure 2. Health degradation can be estimated by trend monitoring systems using post-flight data [1-3]. Since the progression of health degradation is gradual, it is expected that the actual change in health parameters is small over a number of flights. Therefore, the process of estimating health degradation and updating the in-flight diagnostic system needs to be accomplished once per a number of flights. When the updating process is complete, the estimated health condition becomes the new reference baseline for the in-flight diagnostic system, as shown in Figure 3, until the next update process is completed. Through this periodic baseline update, the in-flight diagnostic system can operate in the vicinity of the degraded engine and thus maintain its diagnostic effectiveness.

In this paper, it is assumed that a trend monitoring system, which is capable of estimating engine health degradation (health parameters), is available. Moreover, it is assumed that this trend monitoring system will achieve a certain level of precision in its estimation performance. The rest of the paper focuses on the development, application, and evaluation of the hybrid Kalman filter for in-flight diagnostics.

Figure 1.–Engine Health Degradation.

Development of the Hybrid Kalman Filter for In-Flight Diagnostics

The Kalman filter described in this section has a unique hybrid architecture; it is composed of a nonlinear on-board engine model (OBEM) and piecewise linear state-space models which include Kalman gain matrices. The OBEM is a physics-based model designed to run in real time, while the piecewise linear state-space models are derived off-line from the OBEM at the nominal health baseline. These two main components are merged together to form the "hybrid" Kalman filter (HKF). Based on the residuals generated by the HKF, a fault indicator signal is constructed for diagnostics.

Hybrid Kalman Filter Design

The design steps for the HKF are exactly the same as those for the general linear Kalman filter. First, a nonlinear plant model is linearized at a number of operating points. Then, Kalman gains are computed based on the linear representations of the plant model. When implemented, however, linear models and associated Kalman gains are integrated with the nonlinear plant model. An aircraft gas turbine engine under consideration is represented by a nonlinear model of the following form:

$$\dot{x} = f(x, h, u_{cmd}, e)$$
$$y = g(x, h, u_{cmd}, e) + v \tag{1}$$

where x, h, u_{cmd}, and e represent the vectors of state variables, health parameters, control command inputs, and environmental parameters, respectively. For given input values, the nonlinear functions f and g generate the vectors of state derivatives $\dot{x}$ and sensor outputs y. The sensor outputs are corrupted by the white noise vector v. By linearizing the engine model at a reference health baseline (e.g., nominal health condition) and also at a specific environmental condition, the following state-space equations are obtained:

$$\dot{x} = A(x - x_{ss}) + B(u_{cmd} - u_{ss}) + L(h - h_{ref})$$
$$y - y_{ss} = C(x - x_{ss}) + D(u_{cmd} - u_{ss}) + M(h - h_{ref}) + v \tag{2}$$

where A, B, C, D, L and M are the state-space matrices with appropriate dimensions. The vectors x_{ss}, y_{ss}, and u_{ss} contain the steady-state values at which the nonlinear engine model is trimmed for linearization. The vector h_{ref} represents a reference health baseline. The Kalman gain is computed based on the matrix pair $[A, C]$, and the linear Kalman filter equation is given as follows:

$$\dot{\hat{x}} = A(\hat{x} - x_{ss}) + B(u_{cmd} - u_{ss}) + K(y - \hat{y})$$
$$\hat{y} - y_{ss} = C(\hat{x} - x_{ss}) + D(u_{cmd} - u_{ss}) \tag{3}$$

The vectors $\hat{x}$ and $\hat{y}$ represent the estimates of the state variables and sensor outputs, respectively. The matrix K represents the Kalman gain. In order for the Kalman gain to converge, the matrix pair $[A, C]$ must be observable.

It should be noted that the linear Kalman filter in Equation (3) does not account for the influence of health parameter deviations from the reference health baseline in Equation (2). Since the Kalman filter is designed with some robustness to system uncertainty in the form of process noise, it has robustness to health parameter deviations to some extent. However, the Kalman filter does not have the level of robustness which can handle the full health deterioration that an engine will experience over its lifetime.

One approach to make a Kalman filter robust to health degradation is to estimate the health parameter vector h as done in References [7,8]. If a Kalman filter is able to accurately estimate all of the health parameters in real time, the Kalman filter can adapt itself to operate in the vicinity of the degraded engine. This approach, however, requires the following condition: the number of sensors must be at least equal to the number of health parameters [8]. In general, this requirement is not met for aircraft engines. Moreover, even if this requirement is met and thus all health parameters are estimated, there are various factors that can cause some problem in estimating health parameters with high accuracy. Examples of such factors are improper sensor location for health parameter estimation, existence of biases in sensors and actuators, and inherent model-plant mismatch. Therefore, the adaptation of the Kalman filter to the degraded engine through the real-time estimation of health parameters is a challenging problem.

Because of the necessity to account for health degradation of a real engine, and because of the difficulty in achieving in-flight, real-time adaptation of the Kalman filter through health parameter estimation, an alternative approach must be considered. One approach discussed in References [9,10] is to periodically update the Kalman filter based on the health condition estimated by some other means. Through the health baseline update, the performance of the Kalman filter can be maintained in the presence of health degradation.

The process of health baseline update for the general linear Kalman filter is described in the following four steps: 1) estimate the health degradation, 2) trim the closed-loop engine model at the new reference health baseline (estimated health condition), which should be close to the actual health condition, and generate the steady-state vectors, 3) linearize the open-loop engine model and generate state-space matrices, and then 4) compute the Kalman gain. Step 1 can be done off-line by a trend monitoring system which monitors the engine health degradation over time. Steps 3 and 4 may not be necessary according to Reference [9], but step 2 alone can be a time-consuming, troublesome process, especially when many operating points must be accounted for over the flight envelope.

Thus, it is desirable to simplify the update process in order to make it feasible in the real application environment.

Insight on simplifying the health baseline update process can be found from past studies. Reference [9] indicated that the performance of the linear Kalman filter, when applied to degraded engines, can be improved significantly just by updating the steady-state vectors (x_{ss}, y_{ss}, u_{ss}) to the new values derived at degraded conditions. Moreover, Reference [11] demonstrated that the constant gain extended Kalman filter can operate over a wide operating range despite its simple architecture, which basically combines a nonlinear engine model with a single Kalman gain matrix computed at a single operating point. These studies indicate that the Kalman gain itself is not of primary importance to operate the Kalman filter in the environment where various elements, such as health or flight condition, are changing. Rather, the accuracy of the plant model is of primary importance.

Based on the above knowledge, the HKF is developed by replacing the steady-state vectors of Equation (3) with the following nonlinear OBEM:

$$\dot{x}_{OBEM} = f\left(x_{OBEM}, \hat{h}_{ref}, u_{cmd}, z\right)$$
$$y_{OBEM} = g\left(x_{OBEM}, \hat{h}_{ref}, u_{cmd}, z\right)$$
(4)

where the vector $\hat{h}_{ref}$ represents the health condition estimated by a trend monitoring system, which is updated once per a number of flights. The vector z represents the measured parameters which define the flight condition. By integrating the OBEM and linear state-space matrices, the following hybrid Kalman filter is formed:

$$\dot{\hat{x}} = A\left(\hat{x} - x_{OBEM}\right) + K\left(y - \hat{y}\right)$$
$$\hat{y} = C\left(\hat{x} - x_{OBEM}\right) + y_{OBEM}$$
(5)

In Equation (5), the steady-state vectors which appeared in Equation (3) are replaced by the state variables and engine outputs generated by the OBEM. Furthermore, the control command inputs and associated matrices B and D in Equation (3) do not appear in Equation (5) since the effect of control command inputs is accounted for by the OBEM as seen in Equation (4). The structures of the linear Kalman filter in Equation (3) and the HKF in Equation (5) are shown in Figures 4 and 5, respectively, for a visual comparison. Although the vector z which indicates the flight condition does not appear in Figure 4, this vector will be needed to interpolate the piecewise linear Kalman filters designed over the flight envelope.

There are a few things which should be noted about the hybrid structure. First, the HKF depends on the OBEM but not vice versa. The OBEM runs in parallel with the actual engine at the estimated health condition without receiving any feedback signals from the HKF. Therefore, the numerical stability of the OBEM is not influenced by the performance of the HKF. The objective of the OBEM is to generate simulated state variables and sensor outputs at the estimated health condition. By updating the health condition of the OBEM, its state variables and sensor outputs can be brought close to the values of the degraded engine. Since health condition mismatches still exist between the OBEM and the degraded engine due to estimation errors, sensor output mismatches also exist between them. The objective of the HKF, or specifically its linear component, is to further improve the sensor output matching between its estimates and the measured values through the tuning of the state variable estimates. As long as the OBEM operates in the vicinity of the degraded engine (i.e., health condition estimation errors are small), the HKF will maintain its accurate sensor output estimation performance.

Construction of Fault Indicator Signals

The validation of the Kalman filter estimation performance is generally done by evaluating residuals, or the differences between the measured and estimated sensor output values. If residuals are large, it can be considered that the Kalman filter is generating inaccurate sensor output estimates due to the presence of an anomaly, such as a sensor fault, that was not accounted for in the Kalman filter design. To indicate the presence of a fault, a weighted sum of squared residuals (WSSR) is computed as follows:

$$WSSR_{HKF} = \left(y - \hat{y}\right)^T \Sigma^{-1} \left(y - \hat{y}\right)$$
(6)

where

$$\Sigma = diag\left[\sigma^2\right]$$

The vector σ represents the standard deviation of the sensor measurements. The square matrix Σ normalizes the residual vector $\left(y - \hat{y}\right)$. Since the HKF design discussed in the previous section does not account for the presence of a fault, the value of the fault indicator signal, WSSR$_{HKF}$, should increase when a fault occurs in the system.

In addition to the fault indicator signal generated by the HKF, another signal is generated for diagnosis:

$$WSSR_{OBEM} = \left(y - y_{OBEM}\right)^T \Sigma^{-1} \left(y - y_{OBEM}\right)$$
(7)

The above signal also indicates the existence of a fault; its value will increase when the engine experiences a fault. This signal, however, will be sensitive to not only faults but also anything that causes output mismatches between the engine and the OBEM. Any uncertainty that exists in the real environment, such as unknown dynamic elements and modeling errors, will cause this signal to increase. In contrast, the fault indicator signal generated by the HKF is less sensitive to uncertainty. This is due to the fact that the Kalman filter, in
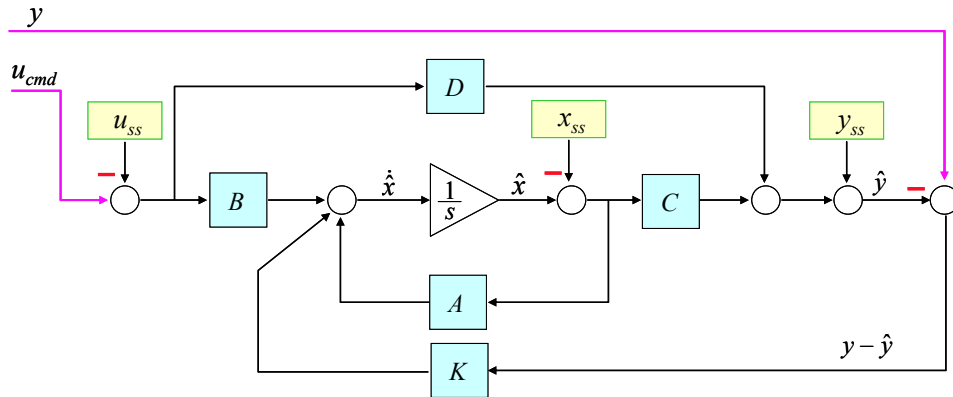
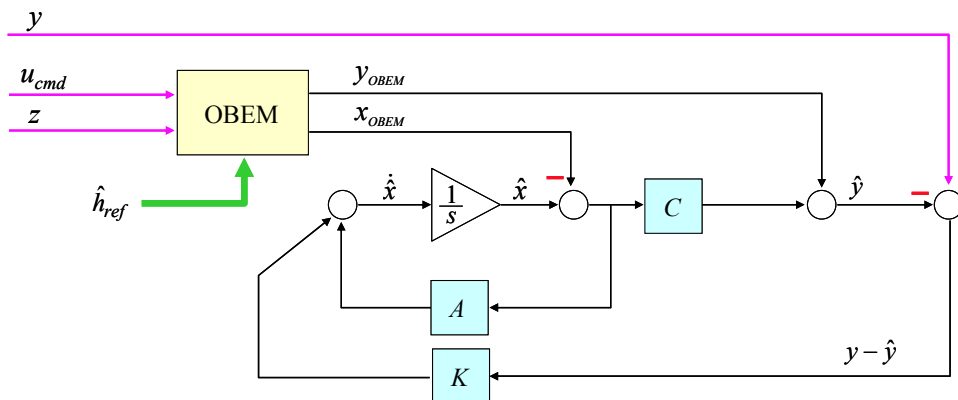Figure 4.–Structure of the Linear Kalman Filter.

Figure 5.–Structure of the Hybrid Kalman Filter.

general, possesses inherent robustness to uncertainty; the process noise used to compute the Kalman gain makes the Kalman filter robust, to some extent. Because of this robustness, the fault indicator signal generated by the HKF may not increase by a significant amount when the engine experiences a fault. The sensitivity of the Kalman filter to faults depends on the sensors being used and also the types of faults. Since the two signals in Equations (6) and (7) have different sensitivity characteristics, both of them are utilized for diagnosis. By using both of them, the effectiveness of engine diagnostics can be improved.

The fault indicator signals are a key element in the in-flight diagnostic process. The first step of the process, the detection of a fault, can be accomplished by comparing the fault indicator signals to a pre-established detection threshold. The establishment of a detection threshold can be based on statistics or achieved through analytical study as was done in Reference

[4]. When a fault indicator signal exceeds the detection threshold, it is considered that a fault indeed exists in the system. Fault detection only reveals the existence of a fault without identifying the specific cause of the detected fault. After fault detection comes fault isolation [9,10] and then fault accommodation [12,13].

Application of the Hybrid Kalman Filter Design Methodology to an Aircraft Engine Model

In this section, the hybrid Kalman filter design technique is applied to an aircraft engine model. Descriptions of the engine model and the engine control are given first, followed by a discussion of the piecewise linear models.

Engine Model

The engine model used in this paper is a nonlinear simulation of an advanced high-bypass turbofan engine, a typical power plant for a large commercial aircraft. This engine model has been constructed as a Component Level Model (CLM), which consists of the major components of an aircraft engine. The CLM represents highly complex engine physics while being designed to run in real time. Engine performance deviations from the nominal health baseline are modeled by adjustments to efficiency and flow capacity scalars of the following five components: Fan (FAN), Booster (BST), High-Pressure Compressor (HPC), High-Pressure Turbine (HPT), and Low-Pressure Turbine (LPT). There are a total of 10 adjustments that are called health parameters. The engine state variables, health parameters, actuator variables, and environmental parameters are shown in Table 1.

There are a total of 11 measured parameters (y and z in Figure 5) that are available to the digital engine control unit of this engine. Table 2 shows seven sensors (y) along with their standard deviations given in percent of steady-state values at the ground maximum power condition. The control actions and diagnostics are based on those sensed variables. Table 3 shows four additional measured parameters (z) along with their standard deviations given in their actual engineering units. These four parameters indicate the ambient and engine inlet conditions. The measurements of the inlet condition, T2 and P2, are used for parameter corrections [14].

The sensor dynamics are currently not modeled; a delay of a single time step is used to represent process delay for each sensor. Similarly, a single-time-step delay is used for the variable geometry actuators (VBV and VSV). For the fuel flow actuator (WF36), a second order dynamic model is used.

The nonlinear engine model is used to represent both the actual engine and the OBEM in the subsequent sections. The engine model representing the actual engine operates at given health conditions, and its flight condition is specified by the three environmental parameters listed in Table 1. The OBEM operates at estimated health conditions, and its flight condition is specified by three measured parameters: T_{amb}, P_{amb}, and T2. From these three measurements, the OBEM calculates the altitude, Mach number, and the temperature deviation from the standard day condition. The actual engine and the OBEM receive the same three control commands (Table 1). However, the WF36 actuator used by the OBEM is represented by a single-time-step delay, whereas a second order dynamic model is used for the engine's WF36 actuator. Typically, there will be a mismatch between the model and the actual engine due to modeling errors and un-modeled elements. The influence of such a mismatch will be assessed in a later section.

Engine Control

The fuel flow controller used in this study has a structure similar to the one described in Reference [15]. It is composed of multiple sub-controllers, each of which computes the rate of change of the fuel flow command based on a specific control objective. The fuel flow rate commands generated by the multiple sub-controllers are processed through the minimum/maximum selection logic. Then, a single control command selected by this logic is fed into a common integrator. The common integrator generates a total fuel flow command input to the WF36 actuator. The current control design is composed of the following sub-controllers:

1) FAN speed control
2) Acceleration and deceleration schedule control
3) Ratio unit (WF36/PS3) control
4) Maximum fan/core speed control
5) Idle control

TABLE 1.–ENGINE MODEL VARIABLES

State Variables	XNL, XNH, TMHS23, TMHS3 TMHSBL, TMHSBC, TMHS41 TMHS42, TMHS5
Health Parameters	FAN efficiency, FAN flow capacity BST efficiency, BST flow capacity HPC efficiency, HPC flow capacity HPT efficiency, HPT flow capacity LPT efficiency, LPT flow capacity
Actuators	WF36, VBV, VSV
Environmental Parameters	Altitude, Mach Number, Ambient Temperature

TABLE 2.–STANDARD DEVIATIONS OF CONTROLS AND DIAGNOSTICS SENSORS (σ IN PERCENT OF STEADY-STATE VALUES AT GROUND MAXIMUM POWER CONDITION)

Sensors (y)	σ (%)
XN12	0.25
XN25	0.25
P25	0.50
T25	0.75
PS3	0.50
T3	0.75
T49	0.75

TABLE 3.–STANDARD DEVIATIONS OF AMBIENT AND ENGINE INLET SENSORS (σ IN ACTUAL UNITS)

Sensors (z)	σ
T_{amb}	5.0 °F
P_{amb}	0.1 psi
T2	5.0 °F
P2	0.1 psi

The positions of the variable geometry actuators (VBV and VSV) are scheduled based on the feedback sensor measurements. In the current control architecture, the power lever angle (PLA) is converted to desired corrected fan speed (an indicator of thrust). The control system adjusts three actuation variables to cause the corrected, measured fan speed to match the desired value. The control system runs with a 0.02-second time step.

Piecewise Linear Model Design

The linear component of the hybrid Kalman filter (A, C, K in Equation 5 and Figure 5) is designed using the nonlinear engine model through the following steps. The nonlinear engine model is first linearized at a number of operating conditions. For each of the linear engine models, a Kalman gain is computed. Then, the piecewise linear models are saved in table lookup form. As the operating condition changes, the piecewise linear models are interpolated based on a scheduling parameter as shown in Figure 6.

The unique aspect of the HKF design is that the piecewise linear models are integrated with the OBEM, instead of the steady-state vectors (x_{ss}, y_{ss}, u_{ss} in Equation 3 and Figure 4) as in the case of a pure piecewise linear Kalman filter design [7,10]. As discussed earlier, having an accurate plant representation is of primary importance in the Kalman filter operation. Because of the use of the nonlinear OBEM which is a good representation of an actual engine, the number of operating conditions at which the piecewise linear models are derived does not have to be as great as for the pure piecewise linear Kalman filter design. In this paper, the piecewise linear models are generated along the steady-state power setting line at a cruise condition. For the interpolation of the piecewise linear models, the estimated corrected fan speed is used as the scheduling parameter. A preliminary study indicated that this

specific HKF design maintains its accurate estimation performance over a wide operating range. When a similar study was done for the HKF using piecewise linear models generated at sea level static condition, the estimation performance was not as good as for the case of cruise condition design. Better estimation performance may be achieved by linking linear models generated at multiple flight conditions, such as climb and cruise. However, it is desirable to keep the dimension of the table lookup as small as possible, since a lesser dimension reduces implementation complexity and also improves execution speed.

When the HKF was implemented in a simulation environment, the system was discretized to run at the frequency of 50 Hz. The parameters used by the HKF algorithm are corrected based on the engine inlet condition T2 and P2.

Evaluation of the Hybrid Kalman Filter

In this section, the functionality of the HKF is investigated using simulation examples. The engine and the HKF are run through a typical flight trajectory which starts from ground idle and continues to takeoff, climb, and cruise. The duration of this flight example is 2500 seconds, and the time histories of three inputs (altitude, Mach number, PLA) are shown in Figure 7.

The estimation accuracy of the HKF is assessed by its residuals ($y - \hat{y}$ in Equation 5) and the fault indicator signal (Equation 6). In addition, the performance of the OBEM is assessed by its residuals and the fault indicator signal (Equation 7). Through the comparison of responses between the HKF and the OBEM itself, the significant contribution made by the linear component of the HKF can be demonstrated.

In the following examples, the health conditions of the engine and the OBEM are set to nominal or degraded conditions. Table 4 shows the degraded health conditions for the engine and the OBEM used in the following examples.

Case 1: Nominal Health Condition

In the first case, both the engine and the OBEM are set to the nominal health condition. This case represents an ideal scenario where no health mismatch exists between the engine and the OBEM. Figure 8 shows the residual responses of the HKF and the OBEM. The residuals shown in the figure have been processed by a low-pass filter with a cutoff frequency of 0.1 rad/sec and also have been normalized by the sensor standard deviations in Table 2. The HKF response is indicated by the solid line while the OBEM response is indicated by the dashed line. Since no health mismatch exists in this case, the outputs of the OBEM match well with the engine outputs. Figure 9 shows the WSSR responses of the HKF (Equation 6) and OBEM (Equation 7). These fault indicator signals have been scaled and also processed by a low pass filter with a cutoff frequency of 0.1 rad/sec. The fault indicator signals are nearly constant throughout the flight except during takeoff. Although
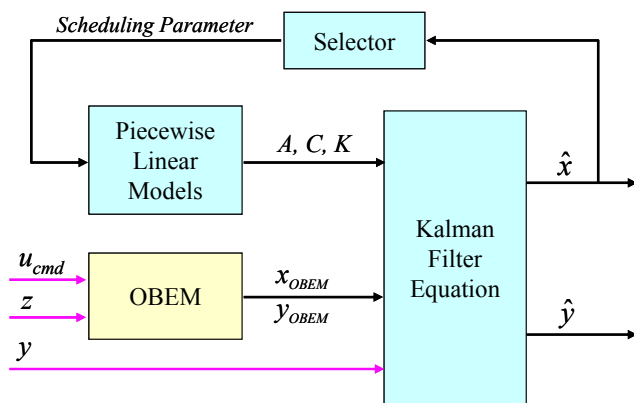

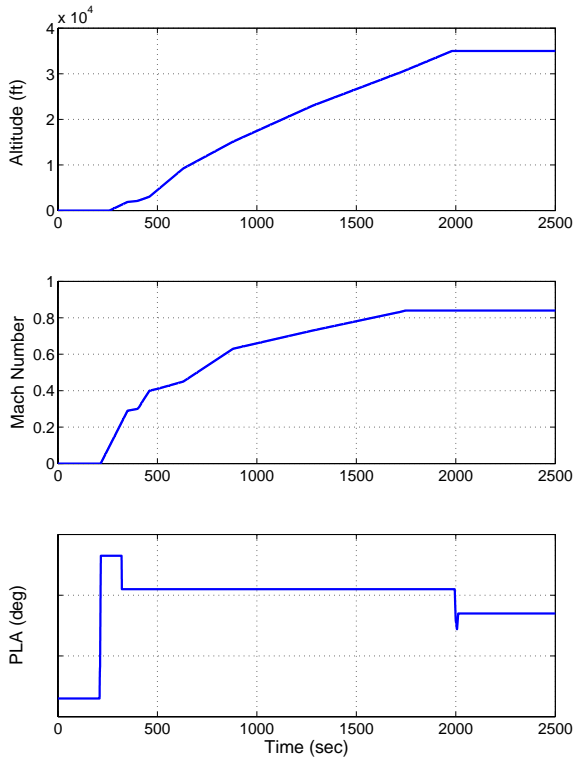Figure 6.–Implementation of the Hybrid Kalman Filter.

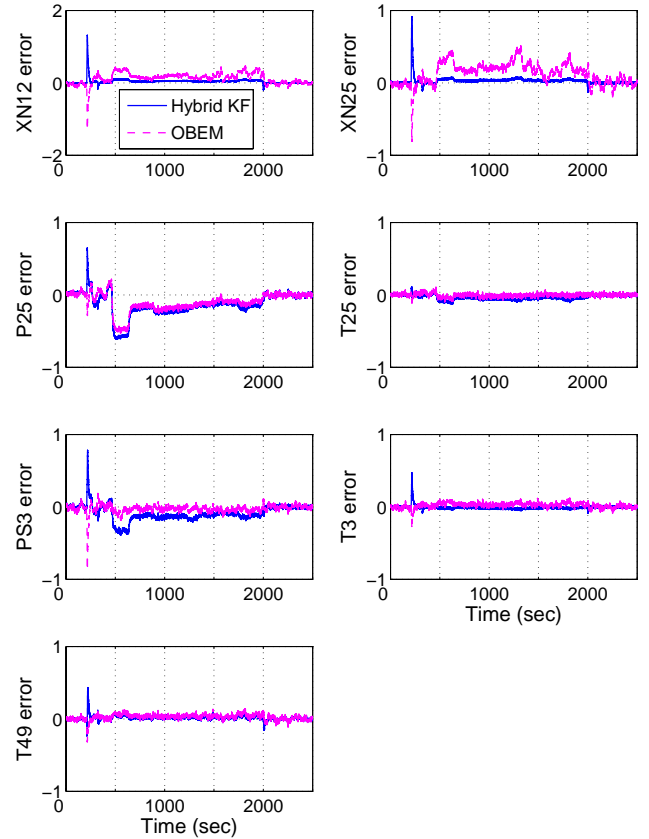Figure 7.–Time Histories of Flight Trajectory Inputs.

Figure 8.–Normalized Residuals of HKF and OBEM at Nominal Health Condition (Case 1).

TABLE 4.–ENGINE HEALTH PARAMETER DEVIATIONS FROM THE NOMINAL CONDITION (CASES 2~4)

	Engine (%)	OBEM (%)	Absolute difference
FAN efficiency	-4.18	-3.72	0.46
FAN flow	-3.09	-2.71	0.38
BST efficiency	-1.69	-1.21	0.48
BST flow	-2.09	-2.33	0.24
HPC efficiency	-4.50	-4.27	0.23
HPC flow	-1.55	-2.03	0.48
HPT efficiency	-4.58	-4.88	0.30
HPT flow	2.19	2.36	0.17
LPT efficiency	-2.14	-2.17	0.03
LPT flow	1.26	1.75	0.49

Figure 9.–WSSR Responses of HKF and OBEM at Nominal Health Condition (Case 1).

the engine and the OBEM are set to the nominal health condition, different WF36 actuator models are used to represent actuator modeling errors as discussed earlier: a second order dynamic model for the engine and a single-time-step delay for the OBEM. This difference causes the spike in WSSR$_{OBEM}$. The spike in WSSR$_{HKF}$ is caused by the delay in the estimation; $\hat{y}$ in Equation (6) lags behind y during major transients such as takeoff.
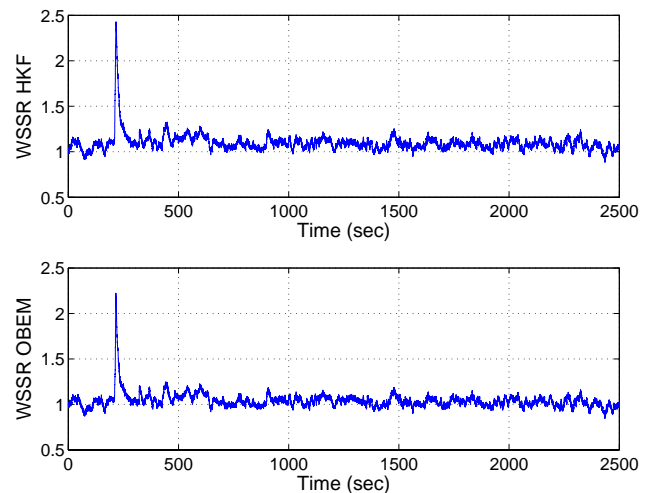
Case 2: Degraded Engine and Nominal OBEM

The second case shows what happens to the estimation performance when the engine is set to the degraded condition shown in Table 4, while the OBEM is set to the nominal health condition. Figure 10 shows the residual responses of the HKF and the OBEM. Because of the large health condition mismatch between the engine and OBEM, the output differences between them are quite large compared to case 1. Moreover, the values of output differences vary along the flight trajectory, whereas they were almost constant in the previous case. However, by comparing the responses of the HKF and the OBEM, it is obvious that the residuals of the HKF are much smaller than the residuals of the OBEM. This is due to the inherent robustness of the Kalman filter technique to uncertainty. The uncertainty in this case is the model-plant mismatch due to health degradation. In the HKF approach, the outputs from the engine and the OBEM are processed with the linear state-space matrices through the Kalman filter algorithm (Equation 5). Through this process, the HKF achieves much better sensor output matching (smaller residuals) than the OBEM. The result of the smaller residuals can be seen in the WSSR responses of the HKF and the OBEM in Figure 11. The WSSR value of the HKF is much smaller than that of the OBEM. It is obvious that the linear component of the HKF plays a significant role in improving the sensor output matching and thus reducing the WSSR value.

Although this improvement is significant, the output differences between the engine and the OBEM are too large in this example; the HKF is unable to maintain its WSSR value at a level comparable to case 1 where both the engine and the OBEM are set to the nominal health condition. Since the linear component of the HKF can only improve the sensor output matching to a limited extent, the health condition mismatch which results in output mismatch between the engine and the OBEM must be maintained within some range. Otherwise, the HKF will generate a large WSSR value, and the degradation will be misinterpreted as a fault.

Case 3: Degraded Engine and Updated OBEM

The previous case showed that a large health condition mismatch between the engine and the OBEM can corrupt the estimation accuracy of the HKF. Thus, the level of such mismatches must be kept within some range so that the HKF will be able to maintain relatively small WSSR values compared to the nominal health case. In this section, the health conditions of the engine and the OBEM are set to the values shown in Table 4. The health condition mismatch between the engine and the OBEM is also shown in the table. The health parameter values of the OBEM were obtained by adding health parameter estimation errors to the health condition of the engine. As discussed earlier, it is assumed that the health condition of the degraded engine is estimated by a trend monitoring system. Its estimation accuracy is assumed to be within ±0.5% from the actual value. The estimation errors
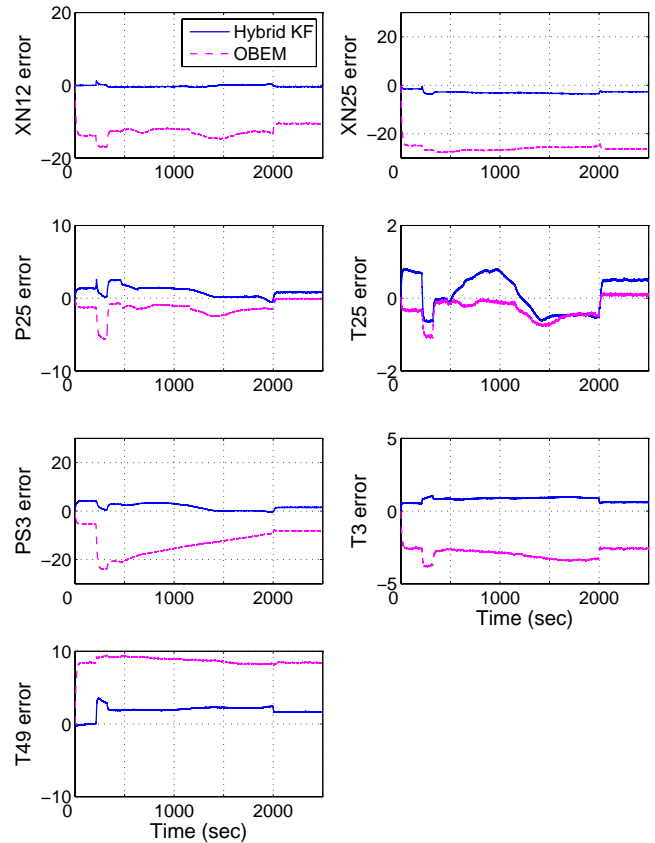

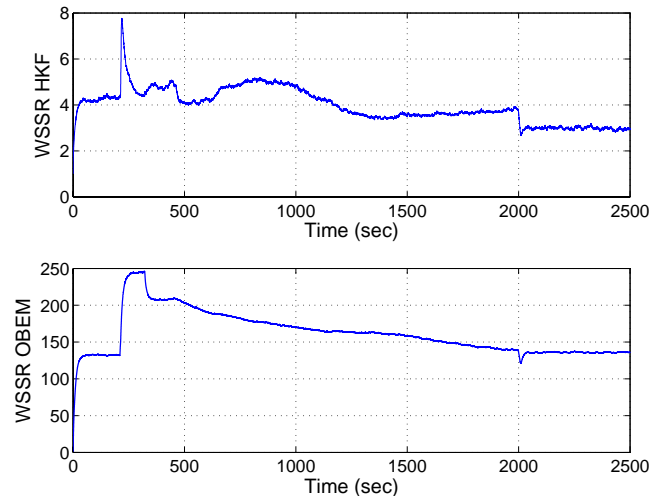Figure 10.–Normalized Residuals of HKF and OBEM Applied to Degraded Engine (Case 2).

Figure 11.–WSSR Responses of HKF and OBEM Applied to Degraded Engine (Case 2).

were generated by a random number generator with uniform distribution over the range of ±0.5%.

Figure 12 shows the residual responses of the HKF and the OBEM. Because of the small health condition mismatch between the engine and the OBEM, the output differences between them are much smaller in this case than the previous one. As was exhibited in the previous case, the HKF performs better than the OBEM; the residuals of the HKF are smaller than those of the OBEM. Figure 13 shows the WSSR responses of the HKF and the OBEM. The WSSR value of the OBEM is still large relative to the value in case 1. However, the WSSR value of the HKF is small and at a level comparable to case 1. Therefore, as long as the health condition mismatch is kept relatively small, the HKF is able to generate accurate sensor output estimates (small residuals), and thus the likelihood of misinterpreting health degradation as a fault can be reduced.

Case 4: Degraded Engine with Unknown Dynamics

In a real implementation, it is unlikely that the real engine is perfectly modeled by the OBEM. Therefore, model mismatch other than a health condition mismatch will exist between the real engine and the OBEM. In this section, the engine and the OBEM are again set to the health conditions in Table 4. In addition to the health condition mismatch, a turbine clearance model, which represents the turbine clearance dynamics with high fidelity, is added only to the engine model representing the real engine in order to introduce unknown dynamics. The presence of the turbine clearance model introduces sensor output mismatches between the engine and the OBEM at steady-state conditions and during transients. Moreover, the level of sensor output mismatches can be varied by setting the turbine clearance condition to specific values.

Figure 14 shows the WSSR responses of the HKF and the OBEM. In this case, the turbine clearance condition is set to nominal. At the nominal clearance condition, sensor output mismatches between the engine and the OBEM are relatively small at steady-state conditions, but they become large during transient operations. Because of the presence of the unknown dynamics in addition to health condition mismatch, the $WSSR_{OBEM}$ value is larger in this case than that of case 3 where there was no turbine clearance model. The $WSSR_{HKF}$ value appears larger than the previous case, especially during takeoff. However, the $WSSR_{HKF}$ value is still relatively small and in the range comparable to case 1. This example shows that the HKF is able to handle not only health condition mismatches but also unknown dynamics such as those introduced through the turbine clearance model.

In the next two examples, the turbine clearance model is operated at off-nominal clearance conditions; sensor output mismatches between the engine and OBEM will be large at steady-state conditions and during transient operations. Figures 15 and 16 show the cases for moderate and large off-nominal clearance conditions, respectively. In Figure 15, it appears the $WSSR_{OBEM}$ value is larger than case 3 (Figure 13) across the flight trajectory. In Figure 16, the $WSSR_{OBEM}$ value is
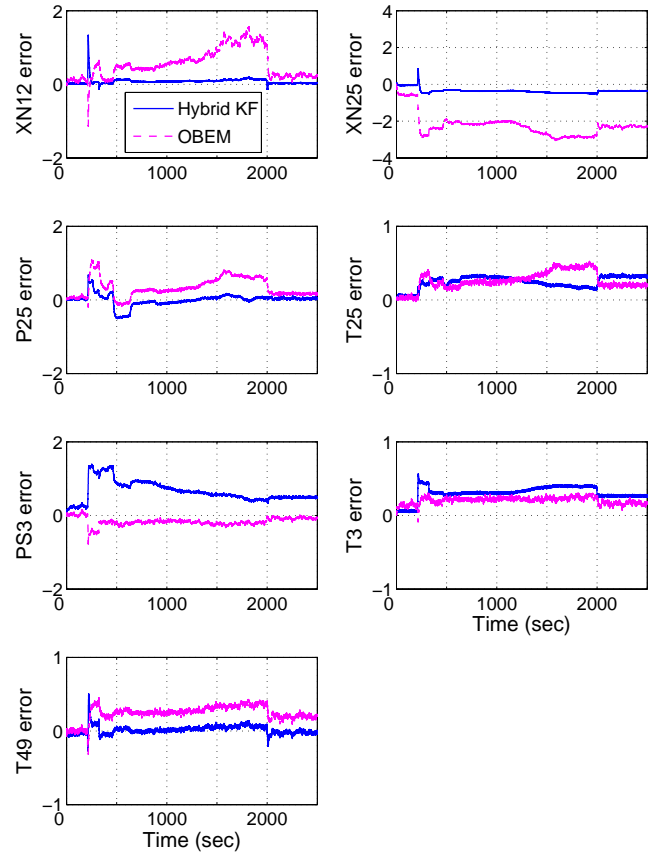

Figure 12.–Normalized Residuals of Updated HKF and OBEM Applied to Degraded Engine (Case 3).
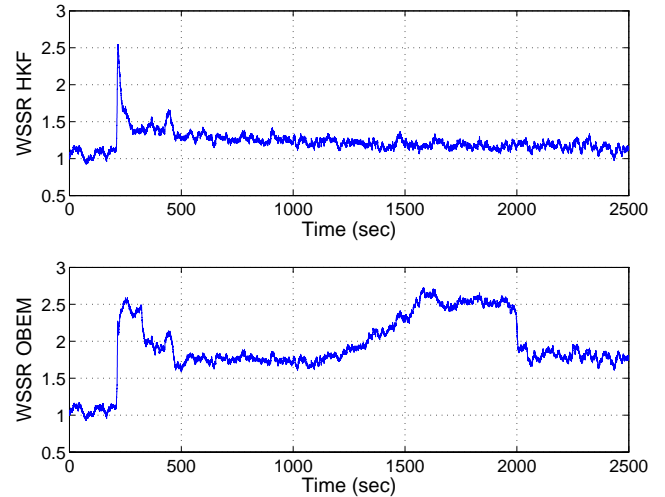

Figure 13.–WSSR Responses of Updated HKF and OBEM Applied to Degraded Engine (Case 3).

significantly larger than case 3 at the ground-idle condition, and there is no sharp rise during takeoff. However, in the rest of the flight trajectory, the $WSSR_{OBEM}$ value remains at a similar level to case 3. Moreover, it can be noticed that the $WSSR_{OBEM}$ value appears smaller than case 3 at the steady-state cruise condition (2000~2500 seconds). It is suspected that, in this specific case, the presence of unknown dynamics counteracts the health condition mismatch, resulting in better sensor output matching between the engine and the OBEM.

Although some variations can be seen during the takeoff segment, the WSSR value generated by the HKF is very consistent throughout the flight trajectory. The $WSSR_{HKF}$ value is also at a level comparable to case 1. Again, these examples show that the linear component of the HKF plays a significant role in the estimation process.

Evaluation Summary

The case studies in this section demonstrate the robustness of the HKF to steady-state and dynamic model-plant mismatch introduced through health degradation and the turbine clearance model. As long as the health condition mismatch between the engine and the OBEM is relatively small compared to the full deterioration range, the HKF is able to generate accurate sensor output estimates, thus maintaining the variation of the $WSSR_{HKF}$ value within a reasonable range. This robustness aspect of the HKF, however, calls into question what will happen to $WSSR_{HKF}$ when the engine experiences a fault. In that case, $WSSR_{HKF}$ must increase by a significant amount to indicate the existence of a fault. Because of the HKF's robustness, it is possible that such a significant increase will not occur, and therefore a missed detection may result. To investigate this issue, the HKF is applied to a fault detection problem in the following section. Two fault indicator signals, one generated by the HKF ($WSSR_{HKF}$) and another generated by the OBEM ($WSSR_{OBEM}$), are utilized to detect faults in sensors, actuators, and components.
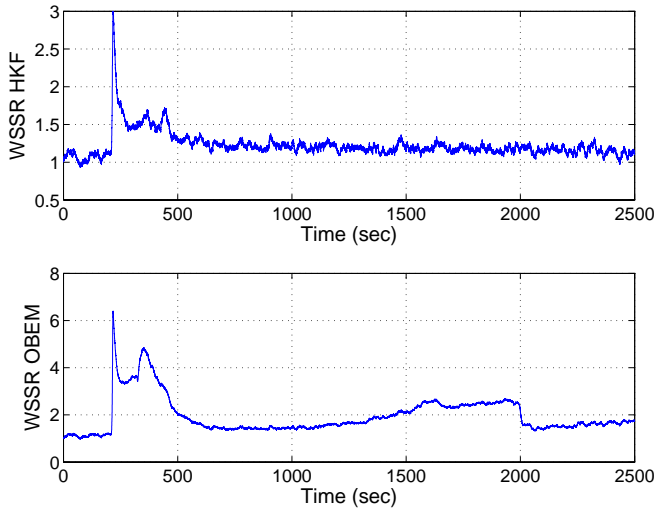

Figure 14.–WSSR Responses of Updated HKF and OBEM Applied to Degraded Engine with Turbine Clearance Model (Case 4 with Nominal Clearance Condition).
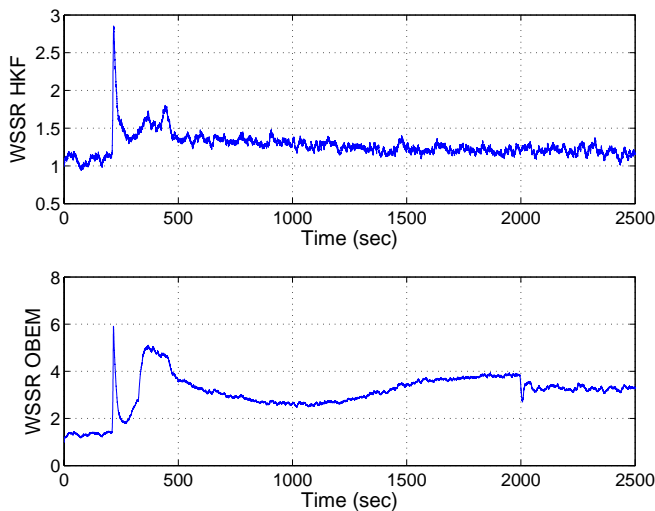

Figure 15.–WSSR Response of Updated HKF and OBEM Applied to Degraded Engine with Turbine Clearance Model (Case 4 with Moderate Off-Nominal Clearance Condition).
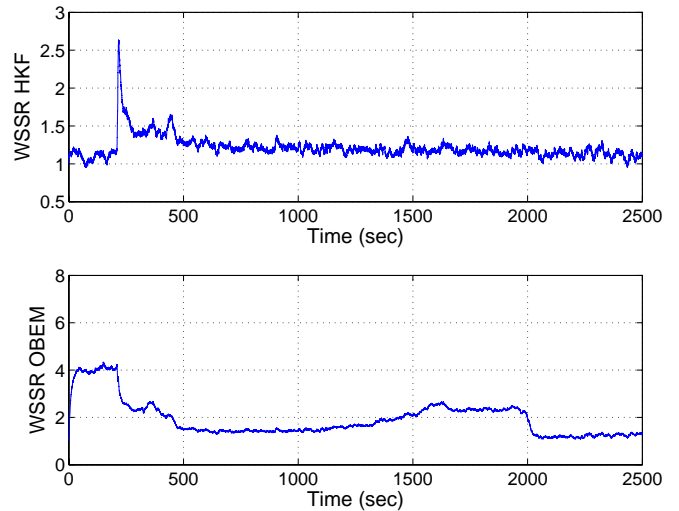

Figure 16.–WSSR Responses of Updated HKF and OBEM Applied to Degraded Engine with Turbine Clearance Model (Case 4 with Large Off-Nominal Clearance Condition).

Application of the Hybrid Kalman Filter for In-Flight Fault Detection

The detection of a fault can be accomplished through the following two steps: 1) generate a fault indicator signal and 2) compare the fault indicator signal to a pre-established detection threshold. When a fault indicator signal exceeds a threshold, it is considered that a fault exists. In the current approach, two fault indicator signals are generated: one from the HKF and one from the OBEM. To detect a fault utilizing these fault indicator signals, the detection threshold must be determined. In this section, the detection threshold is selected for detecting faults at multiple operating points over the flight envelope.

Selection of the Detection Threshold

The selection of the detection threshold value is a critical part in the diagnostic system design. Setting the threshold at a low value increases the chance of detecting faults but also increases the chance of generating false alarms. Conversely, setting the threshold at a high value decreases the chance of generating false alarms but also decreases the chance of detecting faults. As such, the balance between true positive (fault detection) and false positive (false alarms) is adjusted by the threshold. It is statistically impossible to achieve zero false alarm rates while detecting any faults, but the false alarm rate should be maintained acceptably low. Keeping that in mind, the threshold is determined in this section.

A false alarm is the result of misinterpretation of non-fault-related factors which exist in various forms to various degrees. If the influence of such factors on the fault indicator signals is known, a threshold can be derived from that knowledge. Similar to the approach taken in Reference [4], health condition mismatches between the engine and the OBEM are used as an example of non-fault-related factors in order to determine the detection thresholds.

As discussed earlier and demonstrated in the case studies of the previous section, the health baseline of the OBEM must be updated periodically as the health of the real engine degrades gradually with time. However, the health baseline update will never be exact in the real applications, and therefore, health condition mismatch will always exist between the OBEM and the real engine. This mismatch can cause the fault indicator signals to increase. If the threshold is set to higher than the maximum value the fault indicator signals can reach due to health condition mismatch, false alarms can be avoided at least for the case of health condition mismatch.

To investigate the influence of health condition mismatch on the fault indicator signal, 300 cases of health degradation and associated health condition estimates were first generated. Three hundred cases of health degradation were created by randomly shifting all 10 health parameters shown in Table 1. The deviation values were uniformly distributed over the range from 1% to 5%, and this level of deviation is beyond the typical level of engine-to-engine variation due to manufacturing tolerance. Estimated health conditions were created by adding estimation errors to the 300 cases of health degradation. The estimation error for each health parameter was a random number with uniform distribution over the range of ±0.5%. As mentioned earlier, it is assumed that a trend monitoring system is available, and its estimation accuracy is within ±0.5% from the actual values.

Using the above 300 health condition mismatch cases, the engine and the HKF were run for 100 seconds at a steady state operating point defined by the flight condition and the power setting. For each mismatch case, the HKF and the OBEM generated a time history of the fault indicator signals. Then, the maximum value that each of the two fault indicator signals reached during the 100-second steady-state run was saved for each of the 300 cases. Based on the maximum WSSR values for the 300 cases, a histogram was generated to investigate the variation of the fault indicator signals due to health condition mismatch. This process was then carried out at various flight conditions with various power settings. Examples of the histograms generated at three power settings (PLA=65, 70, 75) at a cruise condition are shown in Figures 17 and 18 for the fault indicator signals generated by the HKF and the OBEM. In the current implementation, the fault indicator signals have been scaled and also processed by a low pass filter with a cutoff frequency of 0.1 rad/sec. The arrows in the figures indicate the largest maximum WSSR value among the 300 cases.

From the histograms generated at various operating conditions, it was found that as the power setting increases, the largest maximum WSSR value moves farther to the right in the distribution. This tendency can be seen in Figures 17 and 18. This is due to the fact that, at high power settings, health condition mismatch (as large as ±0.5%) can result in quite large mismatches between the engine and the OBEM state variables and sensor outputs. Under the presence of such large mismatch in sensor outputs, the HKF performs poorly since its linear component can improve the sensor output matching only to a limited extent.

From the above observation, it would be a reasonable approach to use different threshold values at different power settings in order to achieve effective fault detection performance. Therefore, the different threshold values were determined using the histograms generated at various power settings and various flight conditions. For instance, at the cruise condition where the nominal power setting is in the range of 60 to 65 degrees PLA, the threshold values for $WSSR_{HKF}$ and $WSSR_{OEBM}$ are set to 1.6 and 8.0, respectively. At higher power conditions, such as takeoff and climb, larger threshold values are used. It should be noted that the threshold values for $WSSR_{OBEM}$ is set much higher than the threshold values for $WSSR_{HKF}$. This is due to the fact that, as seen in Figures 17 and 18, the $WSSR_{OBEM}$ value is very sensitive to health condition mismatch, resulting in much larger variations than the $WSSR_{HKF}$ value. The threshold values determined at multiple operating conditions are saved in table lookup format and interpolated based on the PLA and altitude.
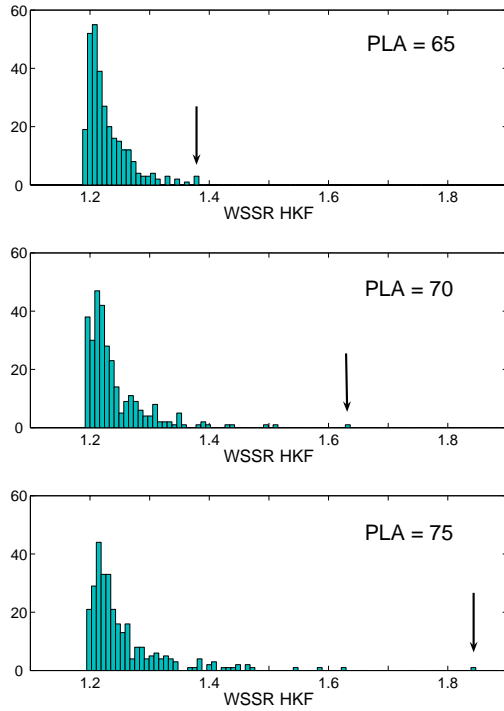
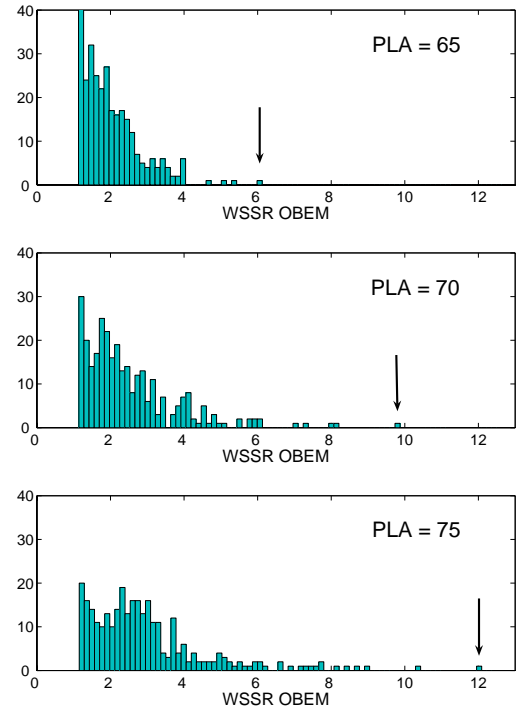Figure 17.–Histograms of Maximum WSSR$_{HKF}$ Values for 300 Health Condition Mismatch Cases at Cruise.

Figure 18.–Histograms of Maximum WSSR$_{OBEM}$ Values for 300 Health Condition Mismatch Cases at Cruise.

Adaptive Threshold

In the earlier section, the influence of unknown dynamics on the fault indicator signals was investigated using the turbine clearance model. By comparing Figures 14 through 16 against Figure 13, it is obvious that the values of the fault indicator signals increase, especially during the rapid transient of takeoff. As such, transient modeling error (unknown dynamics) can cause an increase in the fault indicator signals during transient operations. To ensure that transient modeling error will not cause a threshold violation, an adaptive threshold, which is similar to the one used in References [16,17], is incorporated into the fault detection system. The adaptive threshold used in this study is defined as follows:

$$\gamma = \gamma_{ss} + \gamma_{tran}$$
$$\tau \dot{\gamma}_{tran} + \gamma_{tran} = M_{tran} \tag{8}$$

The adaptive threshold is indicated by γ, whereas the threshold derived in the previous section at various steady-state operating conditions is indicated by γ_{ss}. Another threshold whose value increases during transient operations is indicated by γ_{tran}. This transient threshold is triggered by a parameter M_{tran} which is an indicator of transient operation. When the power setting is at steady-state, M_{tran} is set to the value of 0, and thus the value of the transient threshold remains at 0. When the power setting is moved from one condition to another, M_{tran} is set to a non-zero value. In the current design, the value of the M_{tran} is set to 2.0 for WSSR$_{HKF}$ (Equation 6) and 5.0 for WSSR$_{OBEM}$ (Equation 7). The time constant τ is set to 5.0. These values were determined by running some transient scenarios.

Persistency Test

To further ensure that the threshold violation is due to the existence of a fault, the persistency of threshold violation is checked before declaring the fault. It was determined that the threshold must be violated 25 consecutive time steps (0.5 seconds) to declare fault detection. The steady-state threshold values, adaptive threshold parameters, and persistency test are adjusted based on the engineering judgment of the designer, and the performance of the fault detection system will vary with those design factors.

Overall Architecture of the In-Flight Fault Detection System

The overall architecture of the in-flight fault detection system is shown in Figure 19. The fault detection system is
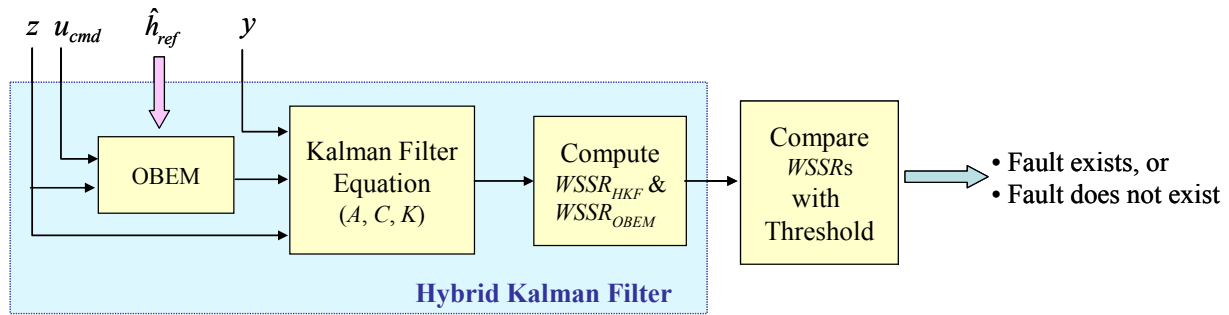
Figure 19.–Overall Architecture of the In-Flight Fault Detection System.

composed of the HKF and the detection threshold. The HKF receives the measured variables (y and z) and control commands (u_{cmd}) from the on-board digital engine control unit, while receiving a periodically updated health baseline ($\hat{h}_{ref}$) from the trend monitoring system. From the HKF and the OBEM, two fault indicator signals, $WSSR_{HKF}$ and $WSSR_{OBEM}$, are generated. Then the two fault indicator signals are compared against the detection thresholds. When at least one of these signals exceeds the threshold for 25 consecutive time steps, the fault detection system declares that a fault exists. It should be remembered that the fault detection system reveals only the existence of a fault, not its identity or severity.

Performance Evaluation of the In-Flight Fault Detection System

In this section, the performance of the fault detection system is evaluated from two aspects: false alarm generation and fault detection. The false alarm aspect is evaluated by running the engine and the fault detection system over a typical fight trajectory in the presence of model-plant mismatch between the engine and the OBEM. The fault detection aspect is evaluated using faults in sensors, actuators, and components.

False Alarm Test

When the fault detection system declares that a fault exists in the absence of actual fault, a false alarm is generated. To investigate the robustness of the system in terms of avoiding false alarms, the fault detection system is run over a typical flight trajectory shown in Figure 7 in the presence of model-plant mismatch.

As shown in Table 5, four scenarios are used in this evaluation. Scenario #1 contains 300 cases of health condition mismatches between the engine and the OBEM. These 300 cases were generated in the earlier section for deriving the detection threshold values. For each case, the health condition

mismatch values are held constant as the engine operates along the typical flight trajectory. In Scenarios #2~4, the same health condition mismatches of Scenario #1 are used. In addition, unknown dynamics (transient modeling error) are introduced in these scenarios through the utilization of the turbine clearance model. In scenario #2, the turbine clearance model is operated at the nominal clearance condition (Figure 14). In scenarios #3 and 4, the turbine clearance model is operated at moderate (Figure 15) and large (Figure 16) clearance conditions, respectively.

Table 5 shows the number of cases for which the fault detection system generated false alarms in each scenario. As can be seen in the table, the turbine clearance model has an obvious impact on the performance of the fault detection system. In a total of 10 cases where false alarms were generated, both fault indicator signals, $WSSR_{HKF}$ and $WSSR_{OBEM}$, exceeded the threshold in two cases. In the rest of the cases, only $WSSR_{OBEM}$ exceeded the threshold. This indicates that the sensitivity of $WSSR_{OBEM}$ to the unknown dynamics is the major contributor to false alarms. To avoid false alarms, the threshold for $WSSR_{OBEM}$ must be set to higher values.

TABLE 5.–FALSE ALARM TEST RESULT

Scenario #	# of Cases	# of False Alarm Cases
1	300	0
2	300	3
3	300	2
4	300	5

Scenario 1: Health condition mismatches.
Scenario 2: Health condition mismatches plus turbine clearance model at nominal clearance condition.
Scenario 3: Health condition mismatches plus turbine clearance model at moderate clearance condition.
Scenario 4: Health condition mismatches plus turbine clearance model at large clearance condition.

Sensor and Actuator Fault Detection

The diagnostic system's ability to detect faults in sensors and actuators is evaluated in this section. A sensor or actuator fault is represented by a bias, and the minimum bias value that can be detected for individual sensors and actuators is determined. This evaluation is conducted at the cruise flight condition, and the PLA is set to 65 degrees. Moreover, the health conditions of both the engine and the OBEM are set to the nominal condition; therefore, there is no health condition mismatch. The engine and the fault detection system are run for 100 seconds at steady-state in the presence of a bias in a single sensor or actuator.

As discussed earlier, a fault is detected when one of the two fault indicator signals exceeds the threshold for 25 consecutive time steps. However, to evaluate the fault detection performance in a relative sense, the following two cases are investigated: 1) fault detection using $WSSR_{HKF}$ alone and 2) fault detection using $WSSR_{OBEM}$ alone. For each case, fault detection is declared when a fault indicator signal exceeds the threshold for 25 consecutive time steps. There are a number of diagnostic approaches for which the OBEM can be utilized. A simplistic approach is to compare the outputs of the engine and the OBEM as done in Reference [18]. The fault detection using $WSSR_{OBEM}$ alone represents this simplistic approach and thus provides a reference performance level that can be achieved when the OBEM is utilized without any estimation algorithm. Relative to this reference performance level, the fault detection using $WSSR_{HKF}$ alone can reveal the performance improvement that can be achieved through the HKF algorithm.

Table 6 shows the minimum bias (both positive and negative) detected for each sensor. The bias values are given in terms of measurement standard deviations. The table indicates that a bias in the P2 sensor is not detected. This sensor is used for the correction of pressure measurements. Since both measured and estimated pressure values are corrected by the P2 value, a bias in this sensor does not increase the residuals.

As can be seen in the table, sensor biases of smaller magnitude can be detected by utilizing $WSSR_{HKF}$ alone. This may appear contradictory to the case studies in the earlier section where the HKF demonstrated its robustness. The Kalman filter is, in general, robust to model-plant mismatch which results in shifts in multiple sensor measurements. However, the Kalman filter is not robust to a sensor bias since it assumes that no bias exists in the system. Conversely, a sensor bias has less influence on the $WSSR_{OBEM}$ value than model-plant mismatch does. When a single sensor is biased, the outputs of the engine and the OBEM remain well-matched, except for only one sensor measurement. A bias in a single measurement is averaged out among the good-matching measurements when $WSSR_{OBEM}$ is computed. As a result, the value of $WSSR_{OBEM}$ is influenced less by a single sensor bias than by model-plant mismatch.

The result in Table 6 reveals the advantage of the HKF algorithm in terms of detecting sensor biases of smaller magnitude; $WSSR_{HKF}$ exceeds the threshold before $WSSR_{OBEM}$ does. When both $WSSR_{HKF}$ and $WSSR_{OBEM}$ are used for fault

TABLE 6.–MINIMUM SENSOR BIAS DETECTED
USING $WSSR_{HKF}$ AND $WSSR_{OBEM}$ INDIVIDUALL
AT CRUISE WITH 65 DEGREES PLA
(NUMBERS IN TERMS OF STANDARD DEVIATIONS)

	$WSSR_{HKF}$ (σ)	$WSSR_{OBEM}$ (σ)
XN12	6.2 / -6.3	6.9 / -6.9
XN25	5.4 / -5.3	6.9 / -6.9
P25	1.8 / -1.8	7.0 / -7.0
T25	2.8 / -2.9	6.9 / -7.0
PS3	2.3 / -2.3	6.9 / -7.0
T3	3.6 / -3.6	6.9 / -7.0
T49	4.4 / -4.4	6.9 / -6.9
T_{amb}	0.4 / -0.5	0.9 / -1.1
P_{amb}	0.7 / -0.6	1.7 / -1.3
T2	0.6 / -0.6	2.0 / -1.5
P2	--- / ---	--- / ---

TABLE 7.–MINIMUM ACTUATOR BIAS DETECTED
USING $WSSR_{HKF}$ AND $WSSR_{OBEM}$ INDIVIDUALLY
AT CRUISE WITH 65 DEGREES PLA
(NUMBERS IN % OF FULL-RANGE VALUE)

	$WSSR_{HKF}$ (%)	$WSSR_{OBEM}$ (%)
WF36	2.4 / -2.3	1.3 / -1.1
VBV	8.9 / ---	22.6 / --
VSV	4.0 / -2.5	3.8 / -2.6

detection as intended, the smaller magnitude biases in Table 6 are detected since only one of the two fault indicator signals needs to exceed the threshold to declare fault detection.

The reader should be reminded that the biases in Table 6 were detected without any health condition mismatch between the engine and the OBEM. As shown in Reference [4], the detected bias values will change when health condition mismatch is introduced.

Table 7 shows the minimum bias detected for each actuator. The bias values are given in terms of percent of the full-range value. As can be seen in the table, the negative bias in the VBV actuator is not detected since this actuator is nearly closed at the cruise condition. The benefit of utilizing $WSSR_{OBEM}$ appears in the case of WF36 bias. Unlike a sensor bias, a WF36 bias results in shifts in multiple sensor measurements. Therefore, through the utilization of $WSSR_{OBEM}$, in addition to $WSSR_{HKF}$, actuator biases of smaller magnitudes can be detected.

Component Fault Detection

The diagnostic system's ability to detect faults in the engine's rotating components is evaluated in this section. A component fault is represented by an abrupt shift in a health parameter. Unlike the sensor/actuator bias case where the engine operates at steady-state in the presence of a bias, the closed-loop engine will undergo transient operation when health parameters are shifted abruptly. After the injection of a component fault, the engine and the fault detection system are run for 100 seconds. When one of the fault indicator signals exceeds the threshold for 25 consecutive time steps, a fault is detected. The evaluation is conducted at the cruise flight condition, and the PLA is set to 65 degrees. Moreover, the health conditions of both the engine and the OBEM are set to the nominal condition.

Table 8 shows the component fault scenarios used to evaluate the fault detection system. There are nine component fault scenarios. Fault scenarios 1 through 5 represent single-component fault cases while fault scenarios 6 through 9 represent multiple-component fault cases. For each fault scenario, four levels of component damage are considered for evaluation. At each damage level, both efficiency and flow capacity of each component are shifted randomly within the range shown in the table. This range is considered to encompass reasonable failure scenarios. All component shifts are made in the negative direction, except for HPT and LPT flow capacities which are shifted in the positive direction. At each damage level of each fault scenario, 100 fault cases are generated by randomly shifting health parameters, thus a total of 3600 component fault cases are used in the evaluation.

Table 9 shows the number of component fault cases detected by the fault detection system. From the table, it can be observed that the performance of the fault detection system varies with the types of component faults. The detection of FAN faults (scenario 1) fails at all damage levels while HPT faults (scenario 4) are detected consistently. This difference is mainly due to the observability of faults through the available sensor measurements. For the FAN component, the shifts in efficiency and flow capacity cause sensor measurement shifts in opposite directions. Thus, when both of them are shifted, the net shift in the sensor measurements remains small. This indicates a different sensor set is needed to successfully detect FAN faults.

The situation where the fault signature (sensor measurement shifts) induced by a health parameter counteracts the fault signature induced by another health parameter seems to occur not only within a single component but also among multiple components. At damage level 1, 98 cases of HPT faults (scenario 4) are detected while 51 fault cases are detected when both HPT and LPT are faulty (scenario 9). At damage level 4, 49 cases of BST faults (scenario 2) are detected, but faults are not detected at all when both FAN and BST are faulty (scenario 6). Successful detection of component faults heavily depends on the available sensors. If different sensor sets are used, different results will be obtained.

It should be noted that different results will also be obtained when the component faults are modeled differently. In the current study, efficiency and flow capacity of each component are shifted randomly within a given damage range, and their shifts are maintained within 1% of each other as shown in Table 8. At the current research level, however, it is not certain how real component faults manifest in the efficiency and flow capacity shifts. It is possible to encounter a component fault of 5% efficiency shift and 1% flow capacity shift. Thus, the result in Table 9 only captures component faults modeled in the described manner.

In this section, both fault indicator signals were used to detect component faults as described earlier. Although the benefit of using $WSSR_{OBEM}$ was not prominent in the sensor fault detection case, an obvious benefit was observed in the component fault case. At damage level 1, all successful fault detection cases of scenarios 4 and 9 in Table 9 were accomplished by $WSSR_{OBEM}$; $WSSR_{OBEM}$ exceeded the threshold while $WSSR_{HKF}$ did not. At damage level 2, $WSSR_{OBEM}$ exceeded the threshold in all successful fault detection cases while $WSSR_{HKF}$ exceeded the threshold only 19 times (all in scenario 4). At damage levels 3 and 4, there were cases where $WSSR_{HKF}$ exceeded the threshold while $WSSR_{OBEM}$ did not. However, it is obvious that the utilization of $WSSR_{OBEM}$, in addition to $WSSR_{HKF}$, results in a benefit of detecting component faults at a higher rate. Again, these fault

TABLE 8.–COMPONENT FAULT SCENARIOS

Fault Scenario #	Faulty Components	Range of Component Damage			
		Level 1	Level 2	Level 3	Level 4
1	FAN	[1%, 2%]	[2%, 3%]	[3%, 4%]	[4%, 5%]
2	BST	[1%, 2%]	[2%, 3%]	[3%, 4%]	[4%, 5%]
3	HPC	[1%, 2%]	[2%, 3%]	[3%, 4%]	[4%, 5%]
4	HPT	[1%, 2%]	[2%, 3%]	[3%, 4%]	[4%, 5%]
5	LPT	[1%, 2%]	[2%, 3%]	[3%, 4%]	[4%, 5%]
6	FAN & BST	[1%, 2%]	[2%, 3%]	[3%, 4%]	[4%, 5%]
7	BST & HPC	[1%, 2%]	[2%, 3%]	[3%, 4%]	[4%, 5%]
8	FAN &BST & HPC	[1%, 2%]	[2%, 3%]	[3%, 4%]	[4%, 5%]
9	HPT &LPT	[1%, 2%]	[2%, 3%]	[3%, 4%]	[4%, 5%]

TABLE 9.–THE NUMBER OF TRUE-POSITIVE
(FAULT DETECTED) CASES AT CRUISE
WITH 65 DEGREES PLA

Fault Scenario #	Level 1	Level 2	Level 3	Level 4
1	0	0	0	0
2	0	0	0	49
3	0	0	11	100
4	98	100	100	100
5	0	7	100	100
6	0	0	0	0
7	0	0	7	100
8	0	0	4	99
9	51	100	100	100

indicator signals have different sensitivities to faults; $WSSR_{OBEM}$ is sensitive to shifts in multiple sensor measurements whereas $WSSR_{HKF}$ is sensitive to shifts in a single sensor measurement. Thus, the benefit of using $WSSR_{OBEM}$ becomes prominent in the component fault case where shifts in multiple sensor measurements are induced. The reader should be reminded again that the fault detection system will not identify the type and severity of a fault; it only indicates that a fault exists.

Remarks on the Hybrid Kalman Filter

The hybrid Kalman filter described in this paper has a unique structure which takes advantage of utilizing the nonlinear OBEM. Because of this structure, the HKF possesses advantages over conventional Kalman filter approaches and is well suited for application to in-flight diagnostics. In this section, some benefits of the hybrid architecture are discussed.

One obvious benefit of the hybrid architecture is that the reference health baseline of the HKF can be updated to the degraded health condition of the engine in a relatively simple manner: by feeding the estimated health condition values to the OBEM. This update process is much simpler than for the case of the pure piecewise linear Kalman filter (PLKF) approach. Without the health baseline update, any in-flight diagnostic system will lose its diagnostic effectiveness as the real engine degrades over its lifetime.

Another benefit is that, in the hybrid architecture, the advantages of the constant gain extended Kalman filter (CGEKF) approach [11,19] and the PLKF approach [10] are combined. The structure of the CGEKF is shown in Figure 20. The advantage of the CGEKF over the PLKF is its capability to capture nonlinear, off-design closed-loop engine operation. Such operation can be described using an example shown in Figure 21. In this figure, the thick solid line indicates the steady-state relationship between the fan speed and the fuel flow. An engine is expected to operate along this steady-state line. Point 1 indicates an "on-design" operating condition at a
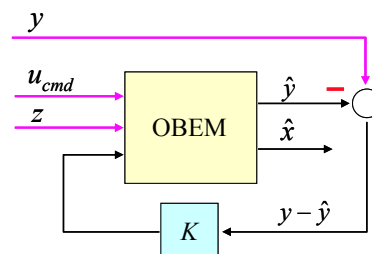

Figure 20.–Structure of the CGEKF.

commanded fan speed. Assume that, at the same fuel flow condition as point 1, the real engine runs at a lower fan speed indicated by point 2. A cause of such deviation from the on-design condition can be a fault, health condition mismatch between the real engine and the expected condition, or other non-fault-related factors (e. g., customer bleeds, horsepower extractions, dirt washout from fan and compressors). If the control objective is to maintain the fan speed at the commanded value, the control system adjusts the fuel flow so that the engine moves to point 3. Depending on the nonlinearity of the closed-loop system, the new operating condition indicated by point 3 may be significantly away from point 1 which is the on-design operating condition at the commanded fan speed. For the case of the PLKF, the steady-state relationships between the parameters are fixed in the steady-state vectors (x_{ss}, u_{ss}, y_{ss}). Therefore, the variation of the steady-state relationships is not captured by the PLKF. On the other hand, the CGEKF and the HKF utilize the nonlinear OBEM in which the nonlinear steady-state relationships between the parameters are embedded. Therefore, the variation of these relationships can be captured by the CGEKF and the HKF.

Although the CGEKF approach has an advantage over the PLKF approach as discussed above, it also has disadvantages in other areas. As noted in Reference [19], the numerical stability of the CGEKF may not be as robust as the PLKF. Since the nonlinear OBEM used in the CGEKF approach receives feedback signals as shown in Figure 20, large residuals may drive the nonlinear OBEM out of the range that the model was
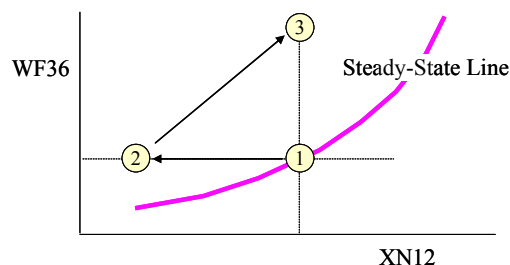

Figure 21.–Nonlinear Engine Operation.

designed for. If this happens even for a short period, the numerical stability of the CGEKF may be lost. On the other hand, in the HKF approach, the numerical stability of the nonlinear OBEM is not influenced by the estimation process since the OBEM does not receive any feedback signals (Figure 6). The OBEM runs as a stand-alone engine simulation, generating state variables and sensor outputs at a given health baseline. Based on the information provided by the OBEM, the Kalman filter algorithm is processed using the piecewise linear state-space models. As such, the HKF possesses the numerical robustness of the PLKF approach and also the nonlinear estimation capability of the CGEKF approach.

Finally, the HKF approach can be easily expanded to a bank of Kalman filters for its application to fault isolation [9,10]. In the hybrid architecture, only the linear component of the filter (A, C, K) must be expanded while using only one OBEM. By combining one OBEM and multiple sets of piecewise linear models, each set being designed based on a unique fault hypothesis, a bank of hybrid Kalman filters can be formed. Therefore, the level of such expansion is similar to the case of the pure PLKF approach.

Conclusion

The hybrid Kalman filter (HKF) approach was developed for its utilization as the core of an aircraft engine in-flight diagnostic system. The HKF has a unique architecture which is composed of a nonlinear on-board engine model (OBEM) and piecewise linear state-space models. In this hybrid architecture, the OBEM functions as an integral part between off-line (non real-time) and in-flight (real-time) diagnostic systems; it operates at a reference health baseline specified by an off-line trend monitoring system, while providing information needed to process the Kalman filter algorithm for in-flight diagnostics. Because of this integration, the in-flight diagnostic system does not need to deal with engine health degradation by itself.

To investigate its capability, the HKF-based fault detection system was evaluated in a simulation environment in the following areas: 1) capability to avoid false alarms and 2) capability to detect faults in sensors, actuators, and components. In the false alarm test, the fault detection system was run over a typical flight trajectory which covered ground-idle, takeoff, climb, and cruise. In this test, the fault detection system demonstrated its robustness in terms of avoiding false alarms in the presence of model-plant health condition mismatch and unknown dynamics. The capability to detect faults in sensors, actuators, and components was demonstrated at a cruise flight condition. The fault detection system was able to detect sensor and actuator biases, but it failed to detect some of the component faults. This shortcoming is mainly due to the limitation imposed by the available sensors, from which fault occurrences are observed. Although fault detection performance can be improved by setting the threshold at a lower value, the false alarm rate will also increase by doing so.

The HKF possesses the combined strength of the conventional linear and nonlinear Kalman filter approaches. The extensive evaluation presented in this paper reveals that the HKF approach is a promising way of implementing the OBEM and the Kalman filter algorithm for real-time, in-flight diagnostics of aircraft gas turbine engines.

Nomenclature

BST	Booster
CGEKF	Constant Gain Extended Kalman Filter
HKF	Hybrid Kalman Filter
HPC	High Pressure Compressor
HPT	High Pressure Turbine
LPT	Low Pressure Turbine
OBEM	On-Board Engine Model
P2	Engine inlet pressure
P25	HPC inlet pressure
P_{amb}	Ambient pressure
PLA	Power Lever Angle
PLKF	Piecewise Linear Kalman Filter
PS3	Combustor inlet static pressure
T2	Engine inlet temperature
T3	Combustor inlet temperature
T49	LPT inlet temperature
T_{amb}	Ambient temperature
TMHS23	BST metal temperature
TMHS3	HPC metal temperature
TMHS41	HPT nozzle metal temperature
TMHS42	HPT metal temperature
TMHS5	LPT metal temperature
TMSHBC	Combustor case metal temperature
TMHSBL	Combustor liner metal temperature
VBV	Variable bleed valve
VSV	Variable stator vane
WF36	Fuel flow
WSSR	Weighted Sum of Squared Residuals
XN12	Fan speed, measured
XN25	Core speed, measured
XNH	Core speed, actual
XNL	Fan speed, actual
e	Environmental parameter vector
h	Health parameter vector
h_{ref}	Reference health condition vector
u_{cmd}	Control command vector
v	Sensor noise vector
x	State variable vector
y	Sensor output vector (controls/diagnostics)
z	Sensor output vector (ambient/engine inlet)

References

[1] Doel, D. L., 1994, "TEMPER – A Gas Path Analysis Tool for Commercial Jet Engines," Journal of Engineering for Gas Turbines and Power, Vol. 116, pp. 82-89.

[2] Volponi, A. J., 1994, "Sensor Error Compensation in Engine Performance Diagnostics," ASME Paper 94-GT-58.

[3] Kobayashi, T., and Simon, D. L., 2005, "Hybrid Neural-Network Genetic-Algorithm Technique for Aircraft Engine Performance Diagnostics," Journal of Propulsion and Power, Vol. 21, No. 4, pp. 751-758.

[4] Kobayashi, T., and Simon, D. L., 2006, "Hybrid Kalman Filter Approach for Aircraft Engine In-Flight Diagnostics: Sensor Fault Detection Case," ASME Paper GT2006-90870.

[5] Mathioudakis, K., and Romessis, C., 2004, "Probabilistic Neural Networks for Validation of On-Board Jet Engine Data," Proceedings of the Institution of Mechanical Engineers, Part G: Journal of Aerospace Engineering, Vol. 218, pp. 59-72.

[6] Romessis, C., and Mathioudakis, K., 2003, "Setting Up of a Probabilistic Neural Network for Sensor Fault Detection Including Operation With Component Faults," Journal of Engineering for Gas Turbines and Power, Vol. 125, pp. 634-641.

[7] Luppold, R. H., Roman, J. R., Gallops, G. W., and Kerr, L. J., 1989, "Estimating In-Flight Engine Performance Variations Using Kalman Filter Concepts," AIAA Paper AIAA-89-2584.

[8] España, N. D., "Sensor Biases Effect on the Estimation Algorithm for Performance-Seeking Controllers," Journal of Propulsion and Power, Vol. 10, No. 4, 1994.

[9] Kobayashi, T., and Simon, D. L., 2003, "Application of a Bank of Kalman Filters for Aircraft Engine Fault Diagnostics," ASME Paper GT2003-38550.

[10] Kobayashi, T., and Simon, D. L., 2005, "Evaluation of an Enhanced Bank of Kalman Filters for In-Flight Aircraft Engine Sensor Fault Diagnostics," Journal of Engineering for Gas Turbines and Power, Vol. 127, pp. 497-504.

[11] Kobayashi, T., Simon, D. L., and Litt, J. S., 2005, "Application of a Constant Gain Extended Kalman Filter for In-Flight Estimation of Aircraft Engine Performance Parameters," ASME Paper GT2005-68494.

[12] Rausch, R., Viassolo, D. E., Kumar, A., Goebel, K., Eklund, N., Brunell, B., and Bonanni, P., 2004, "Towards In-Flight Detection and Accommodation of Faults in Aircraft Engines," AIAA Paper 2004-6463.

[13] Rausch, R. T., Goebel, K. F., Eklund, N. H., and Brunell, B. J., 2005, "Integrated In-Flight Fault Detection and Accommodation: A Model-Based Study," ASME Paper GT2005-68300.

[14] Volponi, A. J., 1999, "Gas Turbine Parameter Corrections," Journal of Engineering for Gas Turbines and Power, Vol. 121, pp. 613-621.

[15] Martucci, A., and Volponi, A. J., 2003, "Fuzzy Fuel Flow Selection Logic for a Real Time Embedded Full Authority Digital Engine Control," Journal of Engineering for Gas Turbines and Power, Vol. 125, pp. 909-916.

[16] Merrill, W. C., DeLaat, J. C., and Bruton, W. M., 1988, "Advanced Detection, Isolation, and Accommodation of Sensor Failures – Real-Time Evaluation," Journal of Guidance, Control, and Dynamics, Vol. 11, pp. 517-526.

[17] Merrill, W. C., DeLaat, J. C., and Abdelwahab, M., 1991, "Turbofan Engine Demonstration of Sensor Failure Detection," Journal of Guidance, Control, and Dynamics, Vol. 14, pp. 337-349.

[18] Healy, T. A., Kerr, L. J., and Larkin, L. J., 1998, "Model Based Fuzzy Logic Sensor Fault Accommodation," Journal of Engineering for Gas Turbines and Power, Vol. 120, pp. 533-536.

[19] Sugiyama, N., 2000, "System Identification of Jet Engines," Journal of Engineering for Gas Turbines and Power, Vol. 122, pp. 19-26.

REPORT DOCUMENTATION PAGE

1. AGENCY USE ONLY (Leave blank)	2. REPORT DATE	3. REPORT TYPE AND DATES COVERED
	December 2006	Technical Memorandum

4. TITLE AND SUBTITLE

Hybrid Kalman Filter: A New Approach for Aircraft Engine In-Flight Diagnostics

5. FUNDING NUMBERS

WBS 645846.02.07.03.03.01

6. AUTHOR(S)

Takahisa Kobayashi and Donald L. Simon

7. PERFORMING ORGANIZATION NAME(S) AND ADDRESS(ES)

National Aeronautics and Space Administration
John H. Glenn Research Center at Lewis Field
Cleveland, Ohio 44135–3191

8. PERFORMING ORGANIZATION REPORT NUMBER

E–15783

9. SPONSORING/MONITORING AGENCY NAME(S) AND ADDRESS(ES)

National Aeronautics and Space Administration
Washington, DC 20546–0001
and
U.S. Army Research Laboratory
Adelphi, Maryland 20783–1145

10. SPONSORING/MONITORING AGENCY REPORT NUMBER

NASA TM—2006-214491
ARL–TR–4001

11. SUPPLEMENTARY NOTES

Takahisa Kobayashi, ASRC Aerospace Corporation, 21000 Brookpark Road, Cleveland, Ohio 44135; and Donald L. Simon, U.S. Army Research Laboratory, Glenn Research Center, Cleveland, Ohio. Responsible person, Takahisa Kobayashi, organization code RIC, 216–433–3739.

12a. DISTRIBUTION/AVAILABILITY STATEMENT

Unclassified - Unlimited
Subject Category: 07

Available electronically at http://gltrs.grc.nasa.gov

This publication is available from the NASA Center for AeroSpace Information, 301–621–0390.

12b. DISTRIBUTION CODE

13. ABSTRACT (Maximum 200 words)

In this paper, a uniquely structured Kalman filter is developed for its application to in-flight diagnostics of aircraft gas turbine engines. The Kalman filter is a hybrid of a nonlinear on-board engine model (OBEM) and piecewise linear models. The utilization of the nonlinear OBEM allows the reference health baseline of the in-flight diagnostic system to be updated to the degraded health condition of the engines through a relatively simple process. Through this health baseline update, the effectiveness of the in-flight diagnostic algorithm can be maintained as the health of the engine degrades over time. Another significant aspect of the "hybrid" Kalman filter methodology is its capability to take advantage of conventional linear and nonlinear Kalman filter approaches. Based on the hybrid Kalman filter, an in-flight fault detection system is developed, and its diagnostic capability is evaluated in a simulation environment. Through the evaluation, the suitability of the hybrid Kalman filter technique for aircraft engine in-flight diagnostics is demonstrated.

14. SUBJECT TERMS

Aircraft engines; Fault detection; Kalman filter; On-board engine model

15. NUMBER OF PAGES

25

16. PRICE CODE

17. SECURITY CLASSIFICATION OF REPORT	18. SECURITY CLASSIFICATION OF THIS PAGE	19. SECURITY CLASSIFICATION OF ABSTRACT	20. LIMITATION OF ABSTRACT
Unclassified	Unclassified	Unclassified	